

# Optical Tag-Based Neuronavigation and Augmentation System for Non-Invasive Brain Stimulation

Xuyi Hu\*

Ke Ma†

Siwei Liu‡

Per Ola Kristensson§

Stefan Goetz¶

University of Cambridge

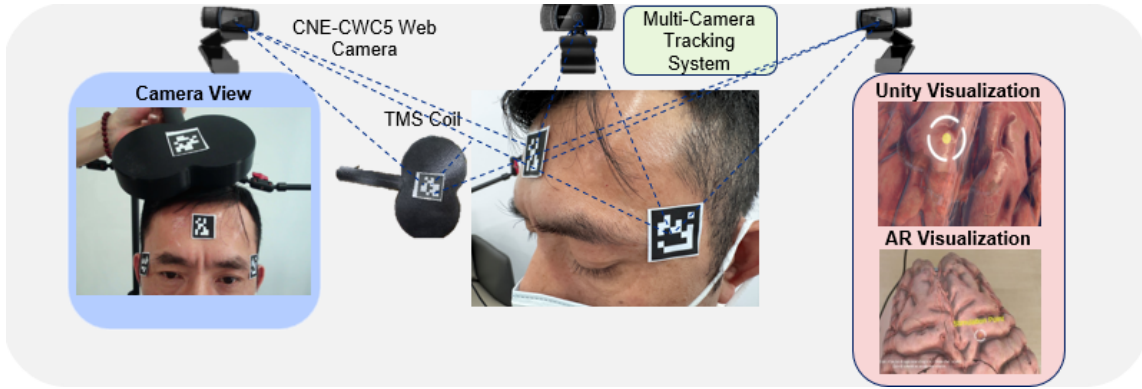


Figure 1: The optical tag-based neuronavigation system combines multi-camera tracking with augmented reality (AR) visualization to improve transcranial magnetic stimulation (TMS) procedures. This system uses low-cost web cameras to track black-and-white optical fiducials on the TMS coil and patient for real-time tracking. Unity 3D visualization and AR overlays guide precise coil positioning and target identification.

## ABSTRACT

Accurate neuronavigation is critical for effective transcranial magnetic stimulation (TMS), as stimulation outcomes depend directly on precise coil placement. Existing neuronavigation systems are often costly, complex, and prone to tracking errors. To address these limitations, we present a computer-vision-based neuronavigation system that enables real-time tracking of the patient and TMS instrumentation. The system integrates a multi-camera optical tracking setup with consumer-grade hardware and visible markers to drive a digital twin of the stimulation process. A dynamic 3D brain model in Unity updates in real time to visualize coil position and estimated stimulation targets. Augmented reality (AR) is further incorporated to project this model directly onto the patient's head, enabling intuitive, in-situ coil adjustment without reliance on abstract numerical displays. Overall, the proposed approach improves spatial precision and accuracy while enhancing usability.

**Index Terms:** Augmented Reality, Computer Vision, Visualization, Neuronavigation, Transcranial Magnetic Stimulation

## 1 INTRODUCTION

An exciting area of augmented reality (AR) is to better support therapy and research on the human brain. Transcranial magnetic stimulation (TMS) is a focal non-invasive technique to write signals into circuits of the brain through strong brief electromagnetic pulses across the intact scalp and skull [3, 20, 38]. In contrast to deep brain stimulation [23, 27], intracortical microstimulation [7, 22], or epidural

stimulation [6], TMS does not require any surgical implantation or even anesthesia. Instead, it works on awake patients. A strong current pulse in a focal stimulation coil generates a local magnetic field [12, 24]. This magnetic field penetrates the scalp as well as skull with minimal distortion and induces a spatially confined electric field in the brain, which in turn depolarizes neurons to respond with so-called action potentials, that is, a neural signal.

TMS is widely used in the treatment of neurological and psychiatric disorders, including depression [26, 31, 40], obsessive-compulsive disorder (OCD) [21, 28], and chronic pain [10, 15, 34]. Cortical mapping and pre-surgical planning locates functions in the brain by sending test pulses and generates maps [16, 17].

Traditional TMS guidance relies on neuronavigation systems based on optical or electromagnetic tracking [13]. Optical systems typically use infra-red stereo cameras to track retroreflective markers, requiring pre-calibration, a restricted operating volume, and uninterrupted line of sight [11, 14]. Guidance is usually presented on external screens, forcing users to interpret numerical data or 3D visualizations from a perspective different from their own, which increases cognitive load and training requirements.

Augmented reality (AR) provides clinicians with intuitive, real-time spatial guidance by overlaying anatomical models or stimulation targets directly onto the patient's head, enabling direct alignment of the TMS coil with cortical targets [9, 30]. This immersive feedback reduces reliance on abstract numerical displays and improves positioning accuracy, usability, and reproducibility. AR has been applied to cortical mapping, pre-surgical planning, and psychiatric neuronavigation, demonstrating its potential to enhance clinical workflows and treatment consistency [33].

Computer vision (CV) promises a non-invasive and cost-effective solution for guiding TMS coil placement. In contrast to the heavy retro-reflective balls, trackers can be simple black-and-white patterns cost-effectively printed onto multiple stickers to be visible from many perspectives. Consumer-grade cameras have reached high resolutions and are readily available to allow multiple cameras from many view points to avoid shadow and perspective problems. Further, multiple cameras can compensate for aberration errors.

\*e-mail: xh365@cam.ac.uk

†e-mail: km834@cam.ac.uk

‡e-mail: sl2049@cam.ac.uk

§e-mail: pok21@cam.ac.uk

¶e-mail: smg84@cam.ac.uk



(a) Tools and targets



(b) Multi-Camera TMS navigation workstation

Figure 2: (a) Components and (b) multi-camera TMS neuronavigation system during experiment. The system consists of a TMS coil, a multi-camera tracking setup for real-time spatial localization, and optical markers attached to the tracked objects and the head for position and orientation detection. The cameras provide synchronized tracking data and translate all components into a unified coordinate frame.

In this paper, we present an AR-enabled neuronavigation system based on printed black-and-white tags, specifically AprilTags, integrated with AR for visualization to enhance accessibility and reduce cost of neuronavigation system (Figure 1). This system leverages CV-based tracking to provide real-time, precise spatial localization of the TMS coil and the patient’s head. The primary contributions of this work are the following:

1. We present a novel low-cost and easy to use tag-based multi-camera neuronavigation system for real-time tracking of TMS coil positioning within 5 mm accuracy at a total cost of £60.
2. We show that the system’s tracking accuracy and effectiveness means this system is practical and competitive compared to existing more expensive neuronavigation methods.
3. We provide integration of a 3D brain model with Unity-based AR visualization, which offers an interactive and easy to use interface for real-time neuronavigation guidance.

## 2 CONVENTIONAL NEURONAVIGATION SYSTEMS

Commercial neuronavigation systems, such as optical and electromagnetic systems, can achieve sub-millimeter accuracy [5, 39], but require substantial financial investment, ranging from \$30,000 to \$100,000 [1, 32]. This results in a high accuracy–cost ratio and limits accessibility. In addition, these systems are complex to operate, requiring extensive training and workflow integration. By contrast, recent advances in consumer-grade cameras enable high-resolution, high-frame-rate visual tracking at significantly lower cost [4, 36].

Previous work has explored TMS coil guidance using marker-based tracking, robotic systems, or mixed-reality visualization. Washabaugh et al. [37] proposed a marker-based approach with acceptable accuracy but limited intuitive feedback and reliance on costly reflective markers. Lin et al. [19] introduced a robotic system for coil alignment, though its expensive hardware and complex setup limit portability. Leuze et al. [18] focused on mixed-reality visualization for intuitive guidance but did not address stimulation target localization. In contrast, our approach avoids specialized tracking hardware or robotics, providing a lightweight, operator-guided solution with real-time visual augmentation for accurate coil positioning.

## 3 TAG-BASED MULTI-CAMERA TRACKING SYSTEM

### 3.1 Tracking Algorithm

Our system uses regular rectangular black-and-white fiducial patterns from the AprilTag family [25, 35]. It consists of high-contrast square patterns that encode unique identification numbers. Further, the sharp edges and the fundamental rectangular grid enable accurate

estimation of location and orientation. The tracking algorithm extracts these markers from camera images, decodes their identities, and determines their 3D position and orientation relative to the camera through perspective transformation.

Tracking based on optical tags with patterns in the visible spectrum provides several advantages over alternative tracking methods. It is computationally efficient and can operate without purpose-designed hardware and instead exploit the latest high-quality low-cost consumer-grade multi-camera and monocular-camera systems.

### 3.2 Multi-Camera Setup

To enable real-time 360° tracking of the TMS coil and patient’s head, we employ a three-camera system that provides continuous spatial localization while minimizing occlusions. Each camera was individually calibrated offline to estimate intrinsic parameters using standard camera calibration procedures. This configuration enables accurate neuronavigation without relying on expensive infrared motion-capture hardware. A shared world coordinate frame is established by combining the fixed geometry of the calibrated cameras with the known spatial arrangement of the head-mounted AprilTag markers. This implicit world anchor enables consistent multi-camera pose estimation without requiring external tracking infrastructure. Each camera captures synchronized frames and independently detects AprilTag markers. Positional information from all views is fused using computer vision to estimate the six-degrees-of-freedom (6 DoF) pose of both the coil and the head. The multi-camera design improves robustness, allowing reliable tracking even when individual cameras experience temporary occlusion. It supports real-time compensation for head motion, making it suitable for practical clinical and research scenarios involving natural patient movement during TMS sessions.

### 3.3 Optical Target Estimation

Accurate target estimation is critical for precise TMS coil placement. We employ a multi-camera tracking system using AprilTag fiducial markers to estimate the poses of the patient’s head and the TMS coil. Five markers are used, with four attached to the head and one to the coil. A global coordinate frame is established by combining the fixed camera geometry with the known spatial arrangement of head-mounted markers, enabling continuous pose estimation under natural head motion and operator hand movement. The multi-camera and multi-marker design provides redundancy, ensuring stable and robust target estimation even under partial occlusion.

#### 3.3.1 Direct Linear Transform

In pose estimation, we aim to determine the rotation and translation that align a known set of 3D points to their corresponding 2D

projections. The transformation from 3D camera coordinates to 2D image coordinates follows the camera projection equation

$$\begin{bmatrix} x \\ y \\ 1 \end{bmatrix} = s \begin{bmatrix} f_x & 0 & c_x \\ 0 & f_y & c_y \\ 0 & 0 & 1 \end{bmatrix} \begin{bmatrix} X \\ Y \\ Z \end{bmatrix} = s \mathbf{K} \begin{bmatrix} X \\ Y \\ Z \end{bmatrix}, \quad (1)$$

where  $f_x, f_y$  are the focal lengths in the  $x$  and  $y$  directions,  $c_x, c_y$  define the optical centre of the camera,  $s$  is depth scale factor and  $\mathbf{K}$  is the intrinsic camera matrix.

### 3.3.2 Pose Estimation

Once a fiducial marker is detected, the algorithm provides the 2D image coordinates of the tag corners. Then, the camera projection matrix as defined in Equation 1 establishes 3D-to-2D correspondences. Given a set of known 3D landmarks (e.g., AprilTag marker corners) and their corresponding 2D image projections, we estimate the camera pose  $\mathbf{R}$  and  $\mathbf{t}$  by solving

$$\min_{\mathbf{R}, \mathbf{t}} \sum_i \left\| \begin{bmatrix} x_i \\ y_i \\ 1 \end{bmatrix} - \pi \left( \mathbf{K} \left( \mathbf{R} \begin{bmatrix} X_i \\ Y_i \\ Z_i \end{bmatrix} + \mathbf{t} \right) \right) \right\|^2, \quad (2)$$

where  $\pi(\cdot)$  is the camera projection function.

### 3.4 Gaussian Error Combination for Increased Precision

After Equation 2, the reprojection error of camera pose  $(\mathbf{r}, \mathbf{t})$  is estimated as follows:

$$e_{\text{proj}} = \frac{1}{N} \sum_{i=1}^N \left\| \mathbf{x}_i - \hat{\mathbf{x}}_i \right\|, \quad (3)$$

where  $\mathbf{x}_i \in \mathbf{R}^2$  is the  $i$ -th corner's detected pixel coordinate, and  $\hat{\mathbf{x}}_i$  is that corner's projected pixel coordinate given the estimated pose.

The uncertainty  $\sigma_{\text{distance}}$  is derived from the re-projection error follows:

$$\sigma_{t_x} = e_{\text{proj}} \frac{t_z}{f_x}, \quad \sigma_{t_y} = e_{\text{proj}} \frac{t_z}{f_x}, \quad \sigma_{t_z} = e_{\text{proj}} \frac{t_z}{\sqrt{f_x^2 + f_y^2}} \quad (4)$$

where  $f_x$  is the camera's focal length in pixels and  $t_z$  is the depth in the camera coordinate system.

The standard deviation for each camera's distance estimate follows:

$$\sigma_{\text{distance}} = \sqrt{\left( \frac{t_x}{d} \sigma_{t_x} \right)^2 + \left( \frac{t_y}{d} \sigma_{t_y} \right)^2 + \left( \frac{t_z}{d} \sigma_{t_z} \right)^2}. \quad (5)$$

When multiple cameras detect the same tag, each camera  $j$  provides distance  $\mathbf{d}$  and standard deviation  $\sigma_{d_j}$ . We combine the distance estimates statistically and consider their variability:

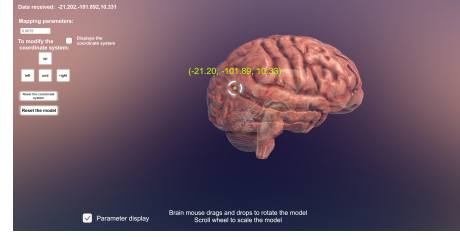
$$d_{\text{fused}} = \frac{\sum_{j=1}^m \frac{d_j}{\sigma_{d_j}^2}}{\sum_{j=1}^m \frac{1}{\sigma_{d_j}^2}}, \quad \sigma_{\text{fused}} = \sqrt{\frac{1}{\sum_{j=1}^m \frac{1}{\sigma_{d_j}^2}}}. \quad (6)$$

Consequently, measurements from more reliable cameras (small  $\sigma_{d_j}$ ) dominate the weighted average, and the resulting fused standard deviation  $\sigma_{\text{fused}}$  reflects the combined confidence.

## 4 EXPERIMENTAL SETUP

### 4.1 Setup

Three cameras are mounted at complementary angles to provide full 3D coverage of the workspace, with one frontal view and two lateral views to maintain visibility of markers on both the head and TMS



(a) 3D Unity brain model.



(b) Augmented-reality neuronavigation.

Figure 3: Visualization of the neuronavigation system. (a) Real-time 3D visualization of the TMS stimulation point integrated with a digital brain model in Unity. (b) Augmented reality interface displaying the stimulation point.

coil. Four  $24 \times 24$  mm AprilTag (tag36h11) markers are attached to the head, with two placed near the cheekbones to minimize the effects of facial muscle movement, and additional markers on the forehead and back. A fifth marker is affixed to the center of the TMS coil for tracking of its position and stimulation point.

We use three commercial cameras (CANYON CNE-CWC5), each with a  $1920 \times 1280$  resolution and a  $65^\circ$  wide-angle horizontal field of view, for experiments. Each camera is priced at £21. The implementation details of the experiment are presented in Figure 2.

### 4.2 Augmented Reality Neuron Navigation System

To enhance the visualization of the targeted brain region during TMS-guided neuronavigation, we first develop a 3D brain model in Unity that dynamically updates to indicate the current stimulation target based on the real-time optical based multi-camera tracking system using the transmission control protocol (TCP). The estimated simulation point is mapped onto the brain model, allowing clinicians to easily visualize the precise location of stimulation in a virtual environment, as shown in Figure 3a.

We integrate AR to project a 3D brain model directly into the real-world environment, enabling intuitive visualization of stimulation targets on the patient's head. AR visualization is implemented using AR Foundation, with tracking data streamed from a PC to an Android device over a local network to ensure real-time responsiveness. Clinicians can thus view and align the TMS coil directly on the patient. The brain model can be either shown alongside the patient or spatially registered and overlaid directly onto the patient's head, and is scaled to match individual head dimensions. Figure 3b illustrates the AR neuronavigation interface, which is demonstrated using an Android smartphone (Xiaomi Mi 9,  $2340 \times 1080$  resolution). By avoiding external monitors or head-mounted AR displays, the system reduces training requirements and supports a more natural, direct view of the stimulation site. This Unity-based AR integration improves usability, accessibility, and precision, making TMS neuronavigation more efficient for clinical practice.

## 5 RESULTS

### 5.1 Precision and Accuracy

The precision and accuracy experiment evaluates the system's measurement stability under identical conditions and its absolute

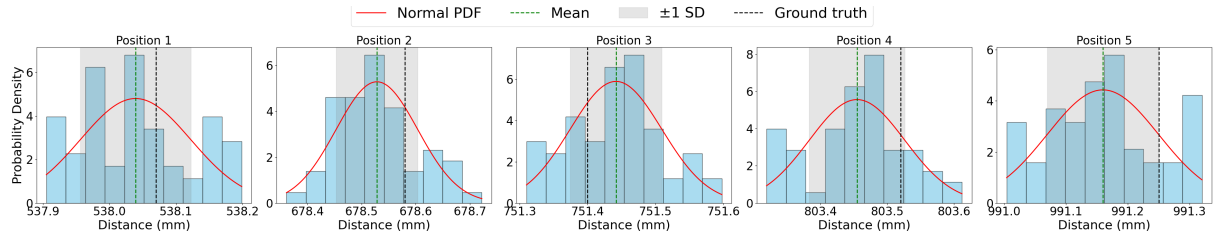


Figure 4: Probability distribution plots of the detected distance in the multi-camera neuronavigation system evaluation across five positions.

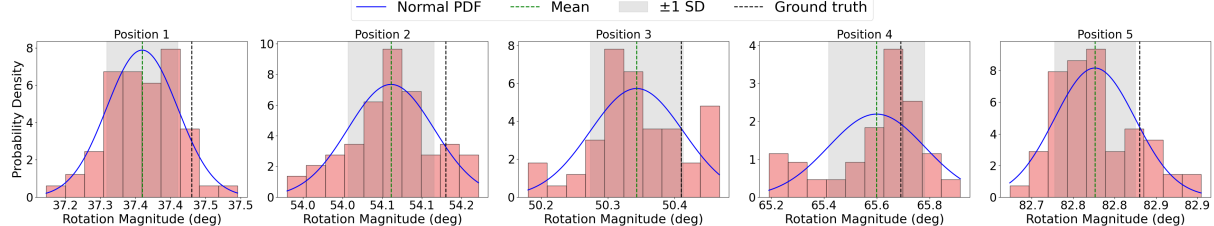


Figure 5: Probability distribution plots of the detected orientation in the multi-camera neuronavigation system evaluation across five positions.

error relative to ground truth. Precision reflects variability across repeated measurements, while accuracy indicates closeness to the true position. Measurements were collected by keeping the TMS coil stationary and recording 100 samples at five positions. As shown in Figures 4 and 5, the proposed multi-camera neuronavigation system demonstrates consistently narrow, near-Gaussian distributions, indicating high precision and stable measurement behavior.

Depth estimation remains stable across all tested distances (approximately 530–990 mm), with standard deviations of 0.07–0.09 mm. Absolute depth errors remain below 1 mm, suggesting robust and accurate distance estimation with only minor deviations attributable to residual calibration or tag detection noise. Rotation measurements exhibit similarly strong consistency, with angular standard deviations of 0.04–0.06° and absolute errors well below 1°. The tight Gaussian fits indicate well-controlled angular noise and reliable orientation estimation across positions.

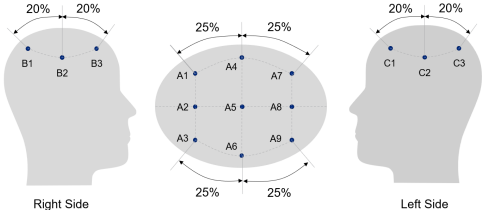
Our system achieves sub-0.1 mm distance precision and sub-0.1° angular precision, with absolute errors below 0.5 mm and 0.3°, respectively. These results confirm the robustness of the multi-camera setup and its ability to deliver high precision and accuracy across diverse measurement conditions.

## 5.2 Stimulation Point Localization Accuracy

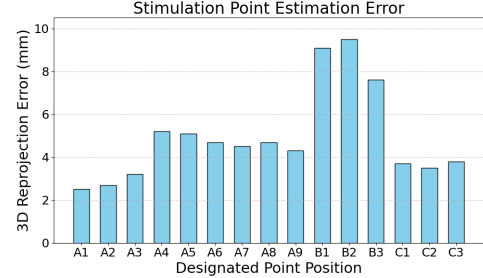
We define our system's accuracy through the Euclidean distance between the estimated 3D position,  $\hat{\mathbf{X}}$ , and the known ground-truth position,  $\mathbf{X}_{\text{true}}$ . The ground-truth positions are known locations measured by optical trackers. Figure 6a shows the location of 15 selected points for accuracy testing and Figure 6b illustrates localization accuracy across 15 different test points.

Figure 6b reveals that the stimulation point estimation error varies across designated positions. This variation in error indicates that there is both systematic bias and random variability in our system. 33.3% of the measurements have errors below 4 mm, 33.3% of the measurements are between 4 and 6 mm, and 16.7% exceed 6 mm.

Figure 7 compares the proposed method with three state-of-the-art neuronavigation systems: Vuforia with HoloLens 1 [8], HoloLens-assisted ventriculostomy [29], and Intel RealSense SR300 [2]. These systems represent marker-based AR tracking, head-mounted AR guidance, and depth-sensing-based tracking, respectively. Our approach and Vuforia HL1 achieve the lowest localization errors, with average errors of 4.94 mm and 3.1 mm, respectively. Both rely on marker-based tracking, which provides stable and reliable performance but requires adequate lighting and unobstructed marker



(a) The positioning of 15 designated TMS stimulation targets for testing.



(b) Bar chart illustrating the stimulation target localization accuracy across 15 different test points. Each bar's height represents the measured 3D re-projection error in millimeters.

Figure 6: Selected stimulation target localization accuracy.

visibility. HL-assisted ventriculostomy shows slightly higher error (5.2 mm), likely due to minor spatial distortions introduced by holographic overlays. Intel SR300 exhibits the largest error (20 mm), reflecting the higher sensitivity of depth-based tracking to lighting conditions, surface properties, and viewing angles. Overall, the results indicate that marker-based approaches offer superior localization accuracy compared to depth-sensing methods, supporting the effectiveness of the proposed system for precise neuronavigation.

## 6 CONCLUSION AND FUTURE WORK

This paper presents an optical tag-based neuronavigation system as a cost-effective and accessible alternative to existing solutions. By using lightweight printed fiducial markers and standard cameras, the system avoids expensive tracking hardware and complex calibration while achieving localization accuracy comparable to state-of-the-art

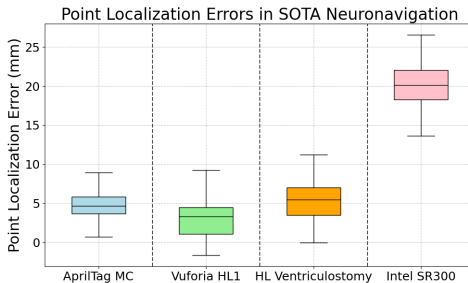


Figure 7: Comparison of point localization errors between state-of-the-art and the presented neuronavigation systems.

methods. The integration of AR visualization further improves usability and spatial awareness, resulting in a neuronavigation approach that is easier to learn and more efficient. Future work will focus on improving robustness under challenging conditions, including variable lighting, rapid motion, and calibration sensitivity. This may be addressed by refining marker detection, enhancing real-time multi-camera calibration, and integrating hybrid tracking that combines optical tags with depth sensing. In addition, Bayesian filtering could be applied to further reduce measurement noise and improve localization accuracy.

## REFERENCES

- [1] Z. K. Asfaw, T. Young, C. Brown, and I. M. Germano. Charting the success of neuronavigation in brain tumor surgery: from inception to adoption and evolution. *Journal of Neuro-Oncology*, 170(1):1–10, 2024.
- [2] M. Asselin, A. Lasso, T. Ungi, and G. Fichtinger. Towards webcam-based tracking for interventional navigation. In *Medical Imaging 2018: Image-Guided Procedures, Robotic Interventions, and Modeling*, vol. 10576, pp. 534–543. SPIE, 2018.
- [3] A. T. Barker, R. Jalinous, and I. L. Freeston. Non-invasive magnetic stimulation of human motor cortex. *The Lancet*, 325(8437):1106–1107, 1985.
- [4] J. Y. Choi, H.-S. Kim, and J. H. Kim. Robust real-time 3d head pose estimation using consumer rgb-d sensors. *Sensors*, 18(3):740, 2018.
- [5] E. R. de Souza Santos, F. R. Viana, P. E. Gonçalves, M. A. C. Lima, C. A. M. Lyra, and B. F. de Oliveira Santos. Precision in neuronavigation systems: A systematic review and meta-analysis. *Arquivos Brasileiros de Neurocirurgia: Brazilian Neurosurgery*, 43(04):e325–e336, 2024.
- [6] V. R. Edgerton and S. Harkema. Epidural stimulation of the spinal cord in spinal cord injury: current status and future challenges. *Expert review of neurotherapeutics*, 11(10):1351–1353, 2011.
- [7] S. N. Flesher, J. L. Collinger, S. T. Foldes, J. M. Weiss, J. E. Downey, E. C. Tyler-Kabara, S. J. Bensmaia, A. B. Schwartz, M. L. Boninger, and R. A. Gaunt. Intracortical microstimulation of human somatosensory cortex. *Science translational medicine*, 8(361):361ra141–361ra141, 2016.
- [8] T. Frantz, B. Jansen, J. Duerinck, and J. Vandemeulebroucke. Augmenting microsoft’s hololens with vuforia tracking for neuronavigation. *Healthcare Technology Letters*, 5:221 – 225, 2018.
- [9] T. Frantz, B. Jansen, J. Duerinck, and J. Vandemeulebroucke. Augmenting microsoft’s hololens with vuforia tracking for neuronavigation. *Healthcare Technology Letters*, 5(5):221–225, 2018.
- [10] R. Galhardoni, G. S. Correia, H. Araujo, L. T. Yeng, D. T. Fernandes, H. H. Kaziyama, M. A. Marcolin, D. Bouhassira, M. J. Teixeira, and D. C. de Andrade. Repetitive transcranial magnetic stimulation in chronic pain: a review of the literature. *Archives of physical medicine and rehabilitation*, 96(4):S156–S172, 2015.
- [11] O. Ganslandt, S. Behari, J. Gralla, R. Fahlbusch, and C. Nimsky. Neuronavigation: concept, techniques and applications. *Neurology India*, 50(3):244–255, 2002.
- [12] S. M. Goetz and Z.-D. Deng. The development and modelling of devices and paradigms for transcranial magnetic stimulation. *International Review of Psychiatry*, 29(2):115–145, 2017.
- [13] S. M. Goetz and Z.-D. Deng. Oxford handbook of transcranial stimulation. *Oxford University Press*, 2021.
- [14] H. K. Gumprecht, D. C. Widenka, and C. B. Lumenta. Brainlab vectorvision neuronavigation system: technology and clinical experiences in 131 cases. *Neurosurgery*, 44(1):97–104, 1999.
- [15] P. Hamid, B. H. Malik, and M. L. Hussain. Noninvasive transcranial magnetic stimulation (tms) in chronic refractory pain: a systematic review. *Cureus*, 11(10), 2019.
- [16] S. M. Krieg, P. Lioumis, J. P. Mäkelä, J. Wilenius, J. Karhu, H. Hannula, P. Savolainen, C. W. Lucas, K. Seidel, A. Laakso, et al. Protocol for motor and language mapping by navigated tms in patients and healthy volunteers; workshop report. *Acta neurochirurgica*, 159:1187–1195, 2017.
- [17] J.-P. Lefaucheur and T. Picht. The value of preoperative functional cortical mapping using navigated tms. *Neurophysiologie Clinique/Clinical Neurophysiology*, 46(2):125–133, 2016.
- [18] C. Leuze, G. Yang, B. Hargreaves, B. Daniel, and J. A. McNab. Mixed-reality guidance for brain stimulation treatment of depression. In *2018 IEEE international symposium on mixed and augmented reality adjunct (ISMAR-Adjunct)*, pp. 377–380. IEEE, 2018.
- [19] Z. Lin, X. Wang, and J. Yang. Trajectory tracking control of robotic transcranial magnetic stimulation. *International Journal of Intelligent Computing and Cybernetics*, 12(2):245–259, 2019.
- [20] S. Liu, B. Wang, K. Ma, X. Hu, L. M. Koponen, A. V. Peterchev, S. M. Alavi, and S. M. Goetz. Prior-information Robbins–Monro sequence for rapid motor thresholding of transcranial magnetic stimulation. *Brain Stimulation: Basic, Translational, and Clinical Research in Neuromodulation*, 18(3):1015–1018, 2025.
- [21] K. Ma, S. W. Chung, and S. M. Goetz. Exploring the dose-dependency of after-effects: A computational model for theta-burst transcranial magnetic stimulation. *bioRxiv*, pp. 2023–07, 2023.
- [22] K. Ma, M. Hamada, V. Di Lazzaro, B. Hand, A. Guerra, G. M. Opie, and S. M. Goetz. Correlating active and resting motor thresholds for transcranial magnetic stimulation through a matching model. *Brain Stimulation: Basic, Translational, and Clinical Research in Neuromodulation*, 16(6):1686–1688, 2023.
- [23] K. Ma, S. Liu, M. Qin, and S. M. Goetz. Extraction of three mechanistically different variability and noise sources in the trial-to-trial variability of brain stimulation. *IEEE Transactions on Neural Systems and Rehabilitation Engineering*, 2024.
- [24] K. Ma, A. Vlasov, Z. B. Simsek, J. Zhang, Y. Li, B. Wang, D. L. Murphy, J. Y. Choi, M. E. Clinton, N. Bukhari-Parlakturk, et al. Optimal asymmetric electric field pulses for selective transcranial magnetic stimulation with minimised power and coil heating. *Brain stimulation*, 2025.
- [25] E. Olson. Apriltag: A robust and flexible visual fiducial system. In *2011 IEEE international conference on robotics and automation*, pp. 3400–3407. IEEE, 2011.
- [26] T. Perera, M. S. George, G. Grammer, P. G. Janicak, A. Pascual-Leone, and T. S. Wilecki. The clinical tms society consensus review and treatment recommendations for tms therapy for major depressive disorder. *Brain stimulation*, 9(3):336–346, 2016.
- [27] J. S. Perlmuter and J. W. Mink. Deep brain stimulation. *Annu. Rev. Neurosci.*, 29(1):229–257, 2006.
- [28] J. L. Rodriguez-Martin, J. M. Barbanjo, V. Perez, M. Sacristan, and C. C. M. D. Group. Transcranial magnetic stimulation for the treatment of obsessive-compulsive disorder. *Cochrane Database of Systematic Reviews*, 2010(1), 1996.
- [29] M. Schneider, C. Kunz, A. Pal'a, C. R. Wirtz, F. Mathis-Ullrich, and M. Hlaváč. Augmented reality-assisted ventriculostomy. *Neurosurgical focus*, 50 1:E16, 2021.
- [30] M. Schneider, C. Kunz, A. Pal'a, C. Wirtz, F. Ullrich, and M. Hlaváč. Augmented reality-assisted ventriculostomy. *Neurosurgical Focus*, 50(1):E16, 2021.
- [31] A. I. Sonmez, D. D. Camsari, A. L. Nandakumar, J. L. V. Voort, S. Kung, C. P. Lewis, and P. E. Croarkin. Accelerated tms for depression: a systematic review and meta-analysis. *Psychiatry research*, 273:770–781, 2019.
- [32] A. J. Sulangi, A. Husain, H. Lei, and J. Okun. Neuronavigation in glioma resection: current applications, challenges, and clinical outcomes. *Frontiers in Surgery*, 11:1430567, 2024.
- [33] B. Wang, A. V. Peterchev, and S. M. Goetz. Three novel methods for determining motor threshold with transcranial magnetic stimulation outperform conventional procedures. *Journal of Neural Engineering*, 20(5):056002, 2023.

- [34] B. Wang, V. Shah, L. M. Koponen, S. M. Goetz, A. D. Neacsu, J. Y. Choi, Z. J. Daskalakis, P. B. Fitzgerald, L. G. Appelbaum, I. Hadas, et al. Stochastic approximator of motor threshold for transcranial magnetic stimulation (samt): Performance in clinical trials. *Brain Stimulation: Basic, Translational, and Clinical Research in Neuromodulation*, 18(4):1291–1292, 2025.
- [35] J. Wang and E. Olson. Apriltag 2: Efficient and robust fiducial detection. In *2016 IEEE/RSJ International Conference on Intelligent Robots and Systems (IROS)*, pp. 4193–4198. IEEE, 2016.
- [36] L. Wang, X. Li, and G. Wang. Pose estimation using consumer-grade rgb cameras: A survey. *IEEE Transactions on Industrial Informatics*, 15(7):3703–3713, 2019.
- [37] E. P. Washabaugh and C. Krishnan. A low-cost system for coil tracking during transcranial magnetic stimulation. *Restorative neurology and neuroscience*, 34(2):337–346, 2016.
- [38] E. Wassermann, C. Epstein, U. Ziemann, V. Walsh, T. Paus, and S. Lisanby. *Oxford handbook of transcranial stimulation*. Oxford University Press, 2008.
- [39] G. H. Yu, C. Park, M. G. Jeong, G. S. Jung, and K. T. Kim. Clinical implementation, barriers, and unmet needs of rtms and neuro-navigation systems in stroke rehabilitation: A nationwide survey in south korea. *Frontiers in Neurology*, 15:1423013, 2024.
- [40] J. Zhou, Y. Wang, X. Luo, P. B. Fitzgerald, R. F. Cash, B. M. Fitzgibbon, and X. Che. Revisiting the effects of rtms over the dorsolateral prefrontal cortex on pain: an updated systematic review and meta-analysis. *Brain stimulation*, 17(4):928–937, 2024.